Title
Fracture Analysis of Drawn Composite Dual Phase Steel Wire

Authors
Sidjanin, L.
Miyasato, S.
Thomas, G.

Publication Date
1987-07-01

Lawrence Berkeley Laboratory
UNIVERSITY OF CALIFORNIA

Materials & Chemical
Sciences Division

To be presented at Interwire '87, Atlanta, GA,
October 25–30, 1987

Fracture Analysis of Drawn Composite Dual-Phase Steel Wire

L. Sidjanin, S. Miyasato, and G. Thomas

July 1987

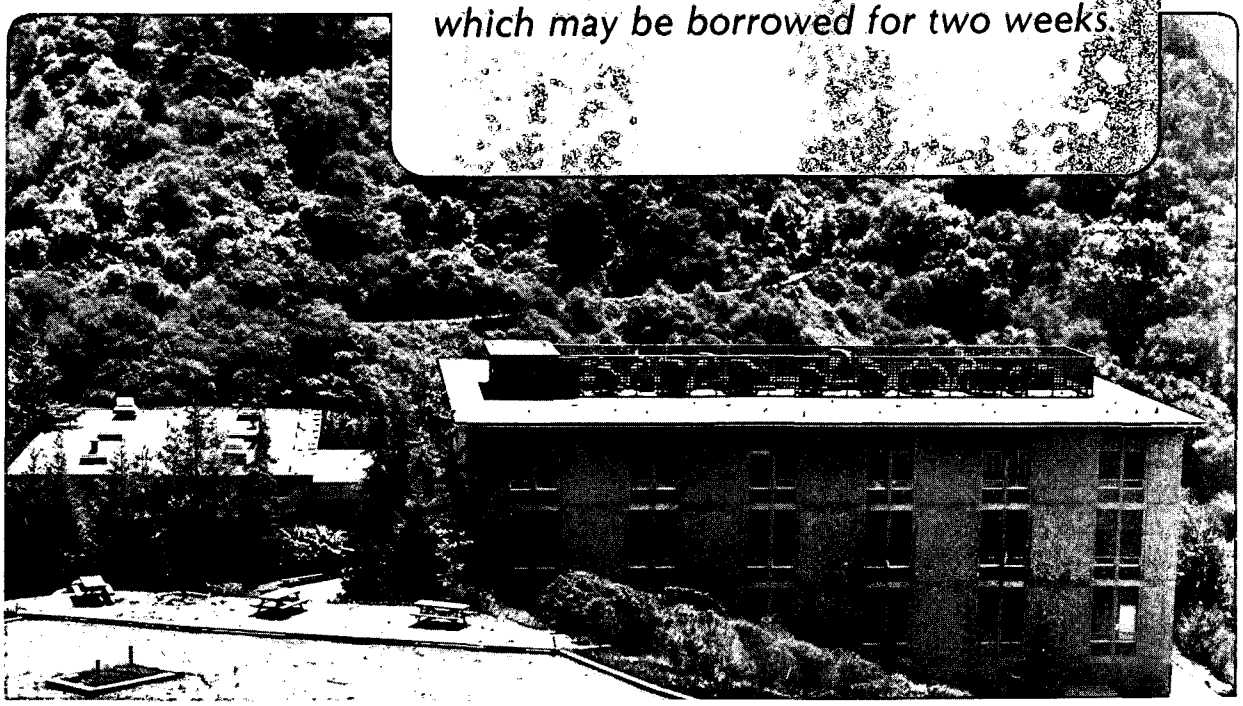

Prepared for the U.S. Department of Energy under Contract DE-AC03-76SF00098

DISCLAIMER

FRACTURE ANALYSIS OF DRAWN COMPOSITE DUAL-PHASE STEEL WIRE

L. Sidjanin*, S. Miyasato and G. Thomas**

Materials and Chemical Sciences Division
Lawrence Berkeley Laboratory
and
Department of Materials Science and Mineral Engineering
University of California
Berkeley, CA 94720

* Fulbright Fellow on leave from the University of Novi Sad, Department of Production Engineering, Faculty of Technical Science, Novi Sad, Yugoslavia

** Professor and Scientific Director of the National Center for Electron Microscopy

DOE contract no. DE-AC03-76SF00098

+ Paper presented at Interwire 87, October 25-30, 1987, Atlanta Georgia

11 Experimental Procedures

The Fe/2 Si/0.1 dual-phase steel (9,10) was used with composition 0.08C, 1.9Si, 0.32 Mn, 0.004P, 0.004S in wt. pct. to develop the dual-phase structure with various morphologies. Thermal and control rolling thermomechanical processing were used as shown in Fig. 1.

The austenitizing time for intermediate quenching (IQ) heat treatment was 30 minutes at 1150°C. After obtaining a fully martensite structure, the specimens were annealed in the ($\alpha+\gamma$), two-phase region for 10 minutes at 910°C and again quenched in agitated ice brine.

The controlled rolling (COR) process employed three steps: rolling in the austenite recrystallization region, rolling in the austenite non-recrystallization region and rolling in the ($\alpha+\gamma$) two-phase region. After finish rolling to final diameter at 910°C, the specimens were directly quenched in agitated iced brine. The intercritical annealing (1A) heat treatment samples were held for 10 minutes at 910°C in the ($\alpha+\gamma$) region and subsequently quenched in iced brine.

Consistent with previous research (17), the temperature in the ($\alpha+\gamma$) region was chosen to be 910°C to maintain the desired 20% volume fraction of martensite which gives the optimum condition for drawability and ductility and to avoid twin plate martensite which is detrimental for drawing (18,19).

The treated samples were machined to 5.5 mm diameter and then drawn without coating in a hand operated drawing machine using 6-8° semi-die angle conical carbide and diamond dies lubricated with Dupont Vydax Freon-Teflon dispersion. The tensile mechanical properties prior to drawing were obtained in an Instron machine and are shown in Table 1.

For wire drawing, the reduction in area per pass in the early stage was 35% and approximtely 20% inthe later states, to a total strain of 5.

The microstructures of longitudinal sections before and after deformation were assessed by light optical and scanning electron microscopy (SEM) using conventional sample preparation methods.

Void density measurements were performed by SEM at 2000X. The measurements were made along the diameter of the wire in two different areas on each given wire size.

111. Results and Discussion

The as-heat treated structures of dual-phase steels are shown in Fig. 2. In these micrographs, the lightly etched phase is martensite and the darkly etched background is ferrite. The volume fraction of martensite for each structure as determined by linear analysis is 20%. Table 1 shows the tensile mechanical properties of the rods prior to drawing. These results are consistent with our earlier studies, e.g., refs. 14-18.

The microstructure obtained by intermediate quenching treatment (IQ) consists of a fine, fibrous distribution of martensite particles in a ferrite matrix, which reflects the influence of the initial martensite structure before two phase annealing. Upon annealing in the ($\alpha+\gamma$) region, the austenite nucleates and grows along the initial martensite lath boundaries forming parallel acicular pools within the prior martensite pocket and then transforms to fine, fibrous martensite upon quenching, Fig. 2a.

The microstructure of the dual-phase steel developed during the controlled-rolling process is shown in Fig. 2b. The initial coarse austentite grains are broken into small recrystallized austenite grains during plastic deformation in the austentite recrystallization region. By continuous deformation at lower temperature, but $>A_3$, the austenite grains are elongated and become the nucleation sites for the transformation of austenite into ferrite. After finish-rolling in the ($\alpha+\gamma$) region and directly quenching, the residual austenite transforms to lath martensite unidirectionally aligned in the fine equiaxed ferrite matrix. The ferrite grain size is finest after this COR treatment.

In the intercritical annealing process the initial microstructure is hypoeutectoid ferrite and pearlite. Upon two-phase annealing, austenite nucleates at carbide-ferrite interfaces and grow, giving rise to the distribution of fine globular martensite along the ferrite boundaries, as shown in Fig. 2c.

The change in morphology of these dual-phase structures as the reduction-in-area by wire drawing was increased is shown in Fig. 3. These micrographs clearly show that void formation during wire drawing occurs in all of the dual-phase microstructures. There exists a linear relationship between the true strain and void density. Figure 4 shows a plot of void density as a function of true drawing strain. It should be noted that Figs. 3 and 4 are compatible. The differences between the drawing limits of the different microstructures is attributed to the differences in void density. The fine fibrous starting microstructure produced by the intermediate quenching process results in a lower void density than that obtained by either controlled-rolling or by intercritical annealing at a given drawing strain.

SEM metallographic examination at high magnification shows that the first voids form in associaion with decohesion along the interface of the small aluminate non-metallic inclusion, i.e., appearing early during plastic deformation. The aluminate inclusions identified by x-ray microanalysis are 2 m in length as shown in Fig. 5.

The great majority of voids are formed at martensite particles either by decohesion of the ferrite/martensite interface or by shear cracking of the martensite particles, Fig. 6. With increasing strain the voids grow longitudinally at the ferrite/martensite interfaces parallel to the direction of the applied drawing load, giving rise to longitudinal microcracks, Fig. 7. Eventually these longitudinal microcracks grow, leading to shear failures and hence limiting the drawability, (e.g., Fig. 8).

The nucleation of voids and microcracks will depend critically on the stress distribution at the ferrite/martensite interfaces and hence on the degree of coherency. Previous high resolution electron microscopy studies (20) have shown dislocated lath martensite to have maximum coherency along the long axes of fibrous particles. These will then be parallel to <110> ferrite directions (20). Clearly shape anisotropy means it is impossible to maintain equivalent crystallographic coherence at all points around the periphery of particles. This is true whether the martensite is in lath form or twin-plate form although the latter morphology is particulary deleterious for formability (14). Consequently, as the stress builds up due to dislocation generation, multiplication, and pile up within ferrite at the ferrite/martensite interfaces, accommodation by plastic flow of the martensite occurs until it itself fractures, or else microcracks must form and will do so at the less coherent interfaces, i.e., at interfaces not parallel to <110> ferrite. This model is consistent with the observations of Fig. 4 and the micrographs, i.e., the poorest drawability occurs with globular martensite morphology (poorest coherence) and the best with the fibrous morphology, since ferrite deforms with the {110}<111> slip systems. Thus a fibrous morphology with axes parallel to interfaces along {110} <111> would clearly be optimum to minimize decohesion and microcracking. This morphology is obtained when Si rather than Mn is used as the principal alloying element (9,10) and so Fe/Si/C rather than Fe/Mn/C dual-phase steels appear to be a better choice for optimum formability and drawability. Also, little benefit seems to be obtained by microalloying elements, e.g., V.

A further point is that decohesion at ferrite/martensite interfaces will be influenced by solute atom segregation. Detailed microanalytical studies (21) show that Mn has a tendency to segregate at these interfaces, but silicon does not.

Thus, economical, simple composition, Fe/Si/C steels treated to obtain fibrous composites of lath martensite in fine grained ($\sim$10μm) ferrite seem to be most promising to obtain high quality wire, e.g., tire cord application, provided casting inclusions are avoided.

IV Conclusions

1. There is a linear relationship between true strain and void density after wire drawing low carbon dual-phase steels for all morphologies studied.

2. Void formation was found to begin either by decohesion of the ferrite/martensite interface, or by shear microcracking of the martensite particles.

3. The formation of voids during wire drawing can be correlated with differences in martensite morphology and hence, martensite/ferrite interface coherency. The fine fibrous starting microstructure produced by the intermediate quenching process results in a lower void density at a given strain, than that obtained by either the controlled-rolling or by the intercritical annealing processes. The worst case is the globular, morphology after the IA treatments.

4. A fibrous distribution of 20% lath martensite in fine grained ferrite appears to be the most promising composite to obtain high strength ductile wire, e.g., for tire cord application and hence Fe/Si/C rather that Fe/Mn/C steels are preferred.

Acknowledgement

This work was supported by the Director, Office of Energy Research, Office of Basic Energy Sciences, Materials Science Division, U.S. Department of Energy under contract No. DE-AC03-76SF00098; partial support of Dr. L. Sidjanin from the Fulbright Program is acknowledged. The authors are grateful to Nippon Kokan K.K., Japan for providing the steels used in this investigation. Thanks are also given to J.H. Ahn for providing some of the wire drawn samples, and for helpful discussions.

References

1. S. Hayami and T. Furukawa; Microalloying 75, Union Carbide Corp., New York, NY (1977), pp. 311.
2. M.S. Rashid; SAE Preprint 760206 G.M. Corp., Warren, MI (1975).
3. Formable HSLA and Dual-Phase Steels, A.T. Davenport, Ed., TMS-AIME, Warrendale, PA (1979).
4. Dual-Phase and Cold Pressing Vanadium Steels in the Automotive Industry, Proc. of Seminar in Berlin, Vanadium Intl. Tech. Comm. (1978).
5. Structure and Properties of Dual-Phase Steels, R.A. Kot and J.W. Morris, Eds., TMS-AIME, Warrendale, PA (1979).
6. Fundamentals of Dual-Phase Steels, R.A. Kot and B.L. Bramfitt, Eds., TMS-AIME, Warrendale, PA (1981).
7. M.S. Rashid and E.R. Cprek; ASTM-STP 647, Philadelphia, PA (1978), pp. 174.
8. J.Y. Koo and G. Thomas, Metall. Trans A, 8A (1977), pp. 525.
9. J.Y. Koo and G. Thomas, Formable HSLA and Dual-Phase Steels, A.T. Davenport, Ed., TMS-AIME, New York, NY (1979), pp. 40.
10. G. Thomas and J.Y. Koo, Structure and Properties of Dual-Phase Steels, R.A. Kot and J.W. Morris, Eds., TMS-AIME, Warrendale, PA, (1979), pp. 183.
11. J.Y. Koo, M.J. Young and G. Thomas, Metall. Trans. A, 11A (1980), pp. 852.
12. N.J. Kim and G. Thomas, Metall. Trans. A, 12A (1981), pp. 483.
13. J.S. Gau and G. Thomas, Metallurgy of Continuous-Annealed Sheet Steel, B.L. Bramfitt and P.L. Mangonon, Eds., TMS-AIME, Warrendale, PA (1982), pp. 333.
14. G. Thomas, Frontiers in Materials Techniques, M.A. Meyers and O.T. Inal, Eds., Elsevier Science Publishers, B.V. The Netherlands (1985), Chap. 3, pp. 89.
15. A.H. Nakagawa and G. Thomas, Metall. Trans.A 16A (1985), pp. 831.
16. J.H. Ahn and G. Thomas, Interwire 85; 55th Annual Convention, Atlanta, GA (1985), pp. 55.
17.J.H. Ahn, Ph.D. Thesis, University of California, Berkeley (1986);LBL-22581.
18. G. Thomas, Mechanical Properties and Phase Transformation in Engineering Materials, R.O. Ritchie and W.W. Gerberich, Eds., S.D. Antolovich, TMS-AIME (1986), pp. 147.
19. G. Thomas, Fundamentals of Microalloying Forging Steel, Eds., G. Krauss and S.K. Banerji, TMS-AIME (1978), pp. 505.
20. J.Y. Koo and G. Thomas, Proc. 35th Annual Meeting, EMSA, Baton Rouge, LA (1977), pp. 118.
21. M. Ohmura, Ph.D. Thesis, University of California, Berkeley (1985), LBL-20530.

Figure Captions

Fig. 1. Schematic diagram to show the thermal and thermomechanical heat treatments used:
a. Intermediate quenching process
b. Controlling rolling process
c. Intercritical annealing process

Fig. 2. Scanning electron micrographs of the dual-phase microstructures obtained after processing:
a. Fibrous martensite produced by IQ- intermediate quenching.
b. Unidirectionally aligned martensite islands produced by COR- controlled rolling.
c. Globular martensite particles produced by IA - intermediate annealing.

Fig. 3. Variation of void density with true strain for different martensite marphologies: A,B,C for IQ; D,E,F for COR; G.H.I for IA with ε=1.20, ε=2.09, and ε=3.58.

Fig. 4. Variation of void density with true strain for different martensite morphologies, IQ, COR, IA with ε=1.20, ε=2.09, and ε=3.58.

Fig. 5. Void initiation and growth occuring on complex aluminate inclusions by decohesion at the inclusion/ferrite interfaces.

Fig. 6. Initiation of voids on martensite particles.
a. Decohesion at the martensite/ferrite interface.
b. Shear cracking of the martensite particle.

Fig. 7. Initiation (A), growth (B), and formation of a longitudinal crack (C), along a martensite/ferrite interface.

Fig. 8. Fracture mode caused by shear instability as an indication of drawing limit.

Table 1. TENSILE PROPERTIES

	σ_Y ksi (MPa)	σ UTS ksi (MPa)	Elongation (%) Uniform	Elongation (%) Total	RA (%)
IQ	72 (496)	118 (814)	13.9	25.2	58
COR	76 (524)	123 (849)	10.2	21.1	57
IA	71 (490)	120 (827)	10.5	19.3	57

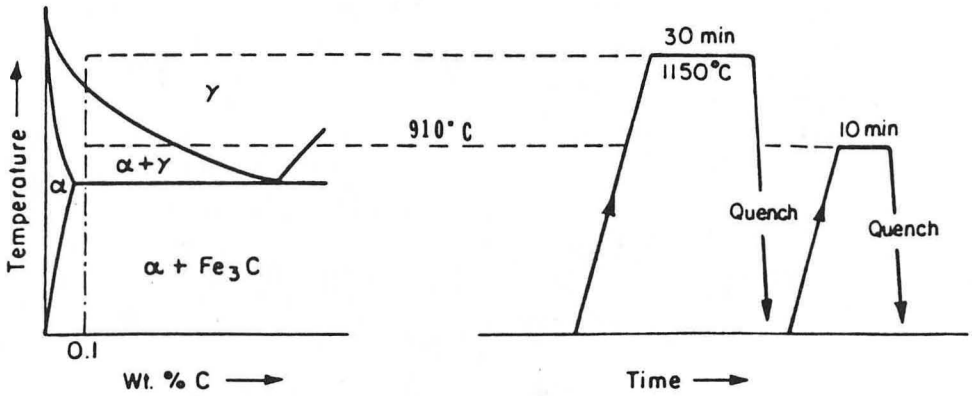

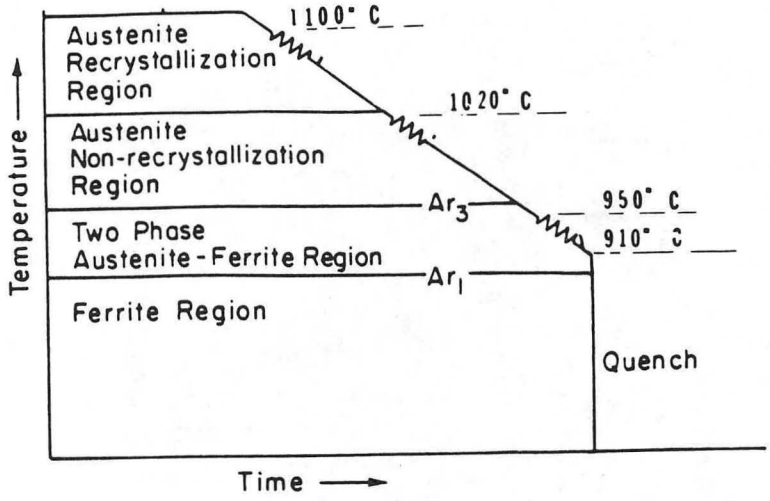

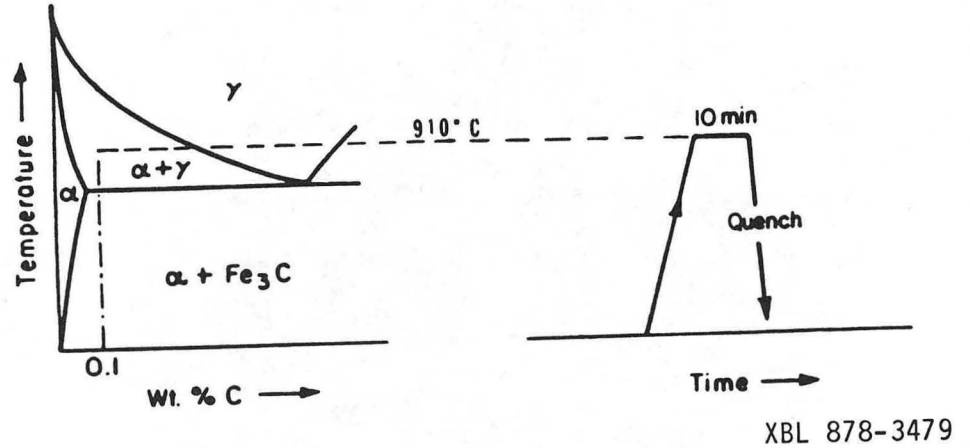

XBL 878-3479

A. Intermediate Quenching Process

B. Controlled Rolling Process

C. Intercritical Annealing Process

Fig. 1

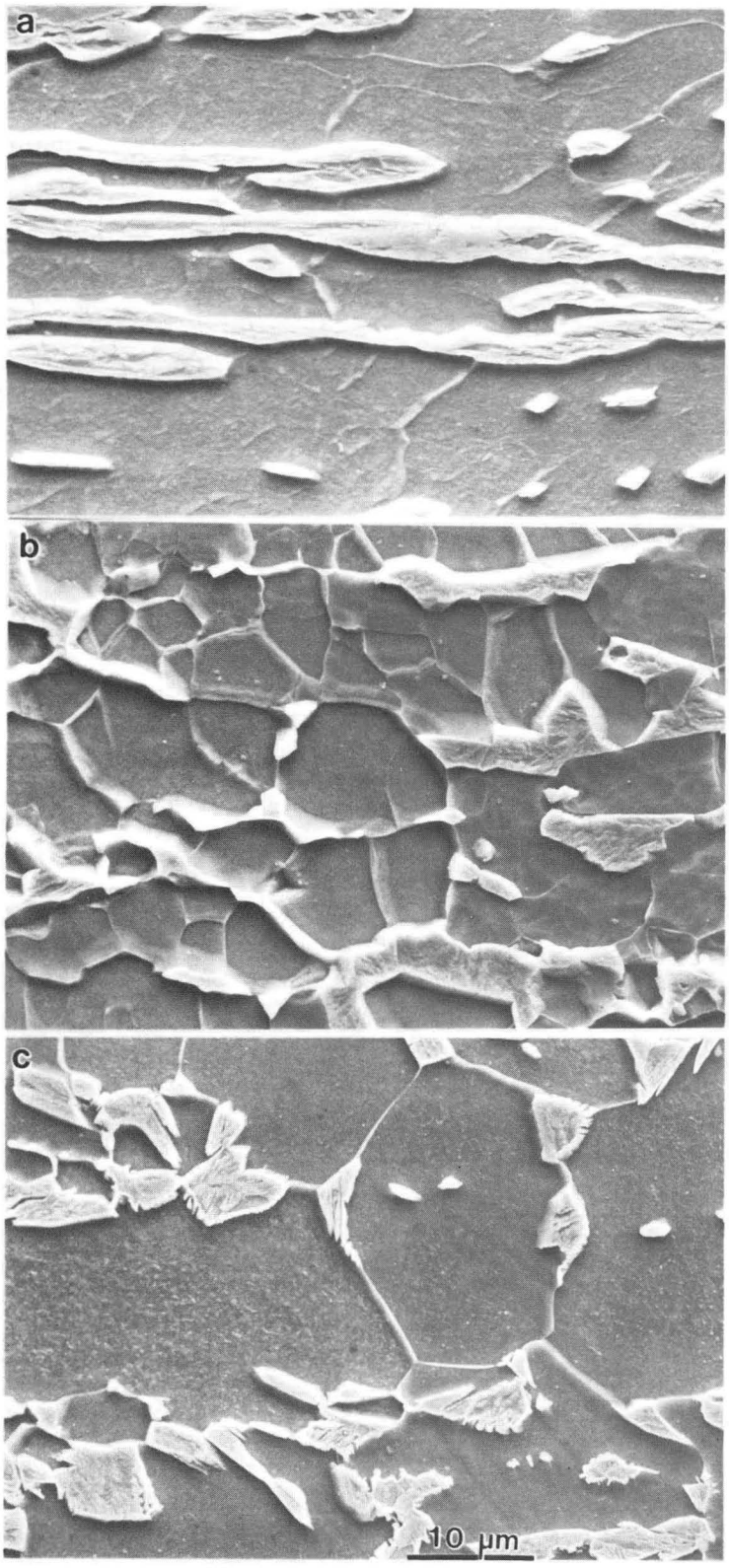

Scanning electron micrographs of the initial dual-phase microstructure produced by
a) IQ - intermediate quenching,
b) COR - controlled rolling, and
c) IA - intercritical annealing.

Fig 2

XBB 876-4847

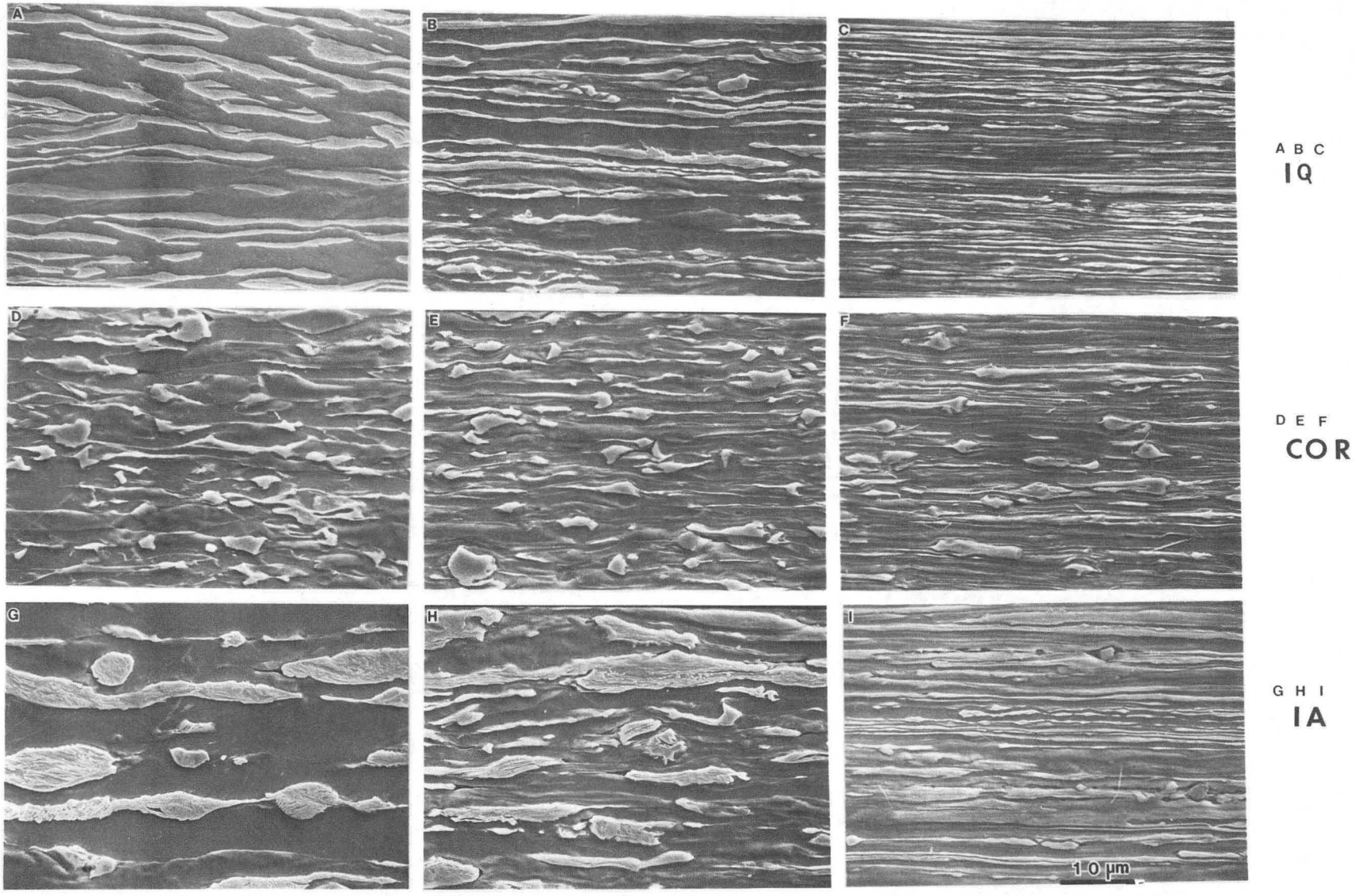

Variation of void density with true strain
for different martensite morphologies.

Fig 3

XBB 875-3834

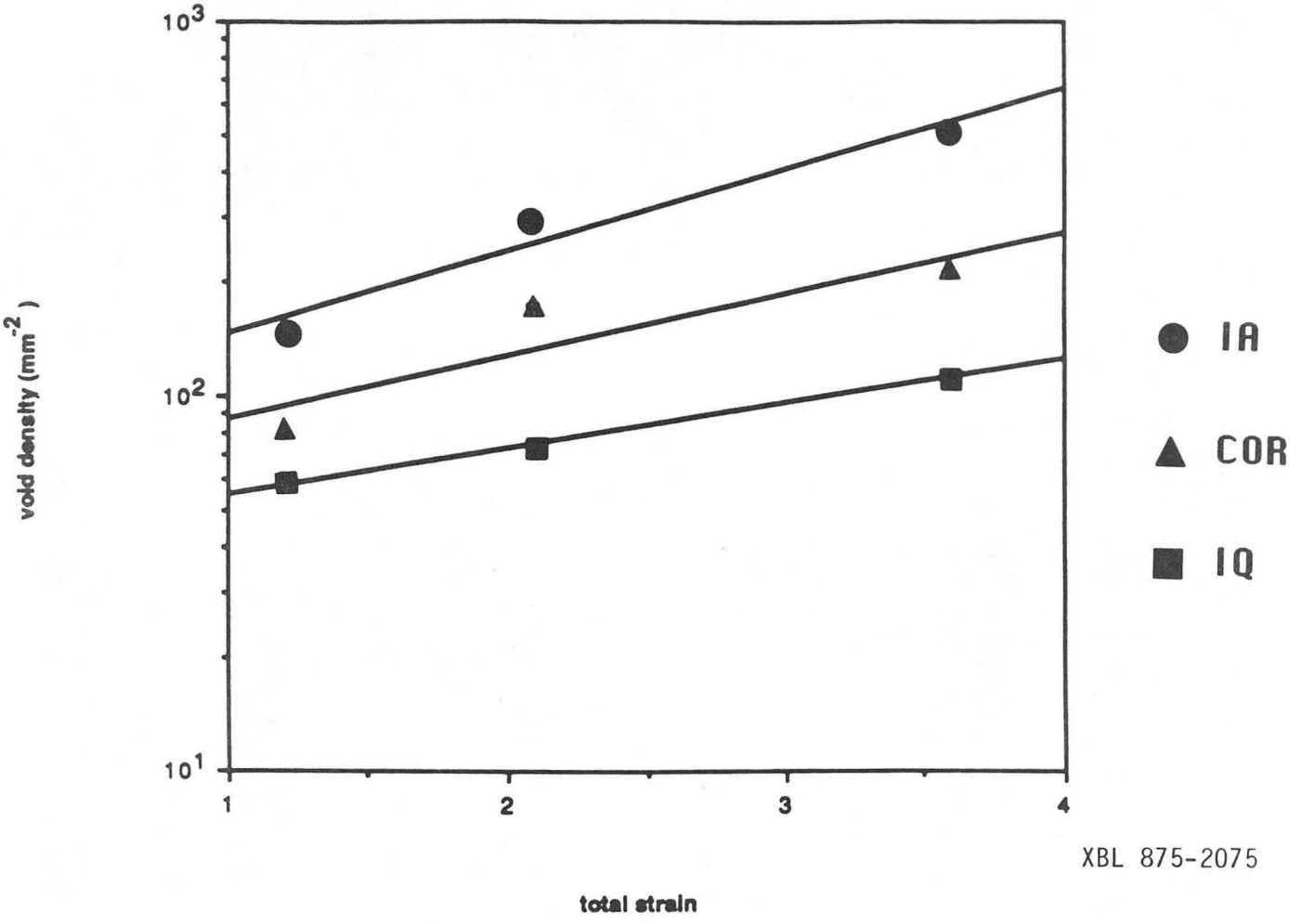

Variation of void density with true strain
for different martensite morphologies.

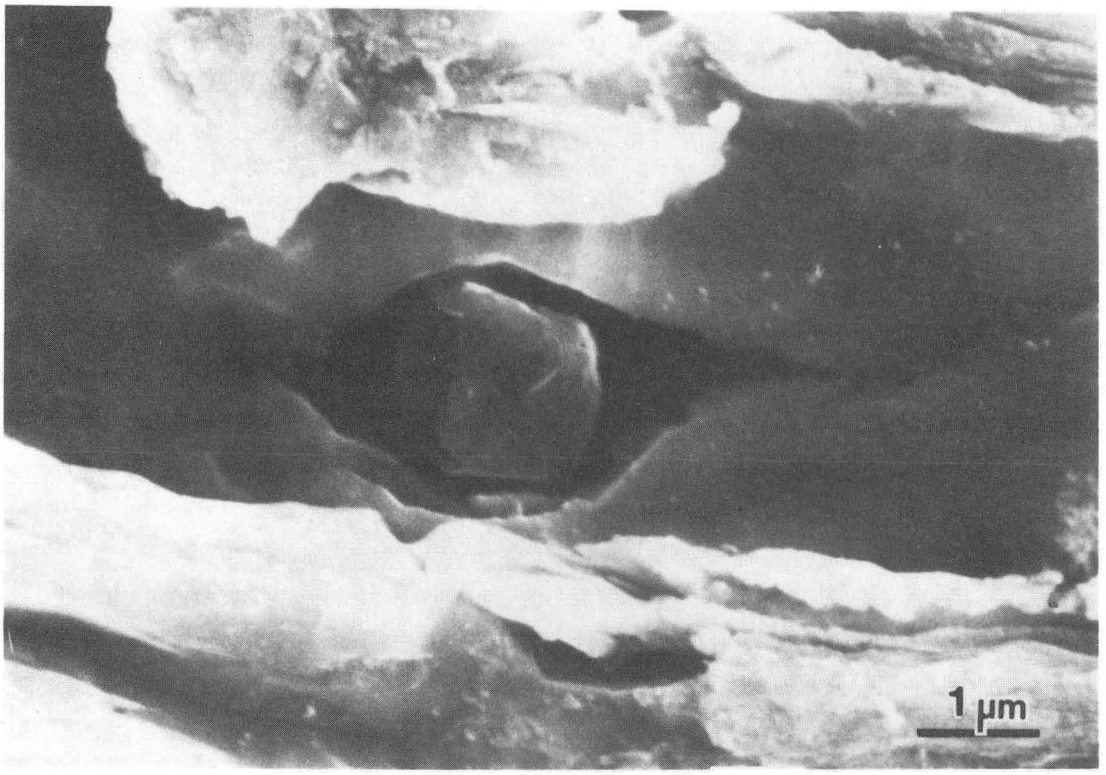

$\varepsilon = 1.20$

XBB 878-6574

The void on complex aluminate inclusion

Fig 5

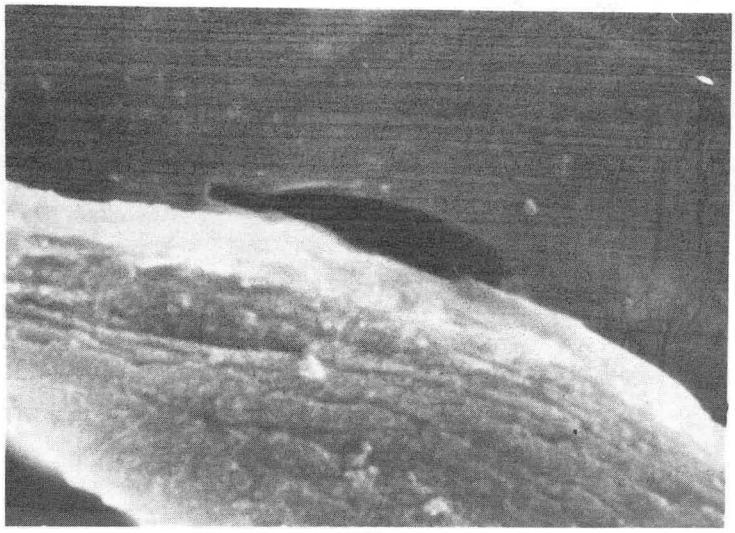

ε = 1.20

A. Decohesion

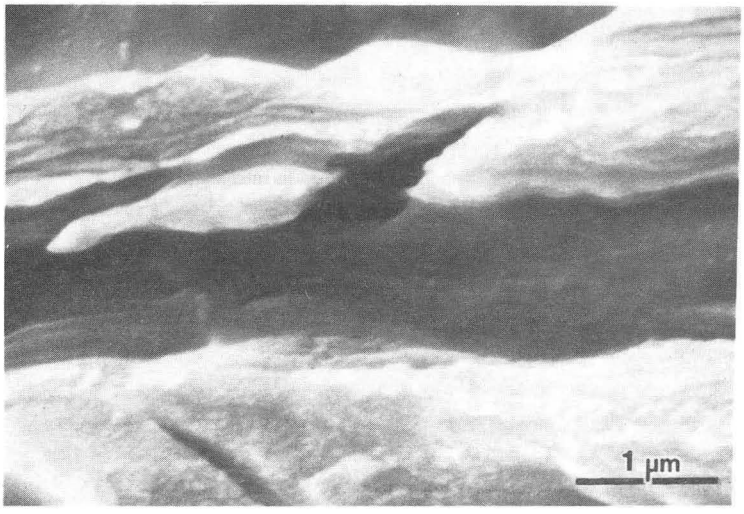

ε = 2.09

B. Shear Cracking

XBB 878-6575

Fig 6

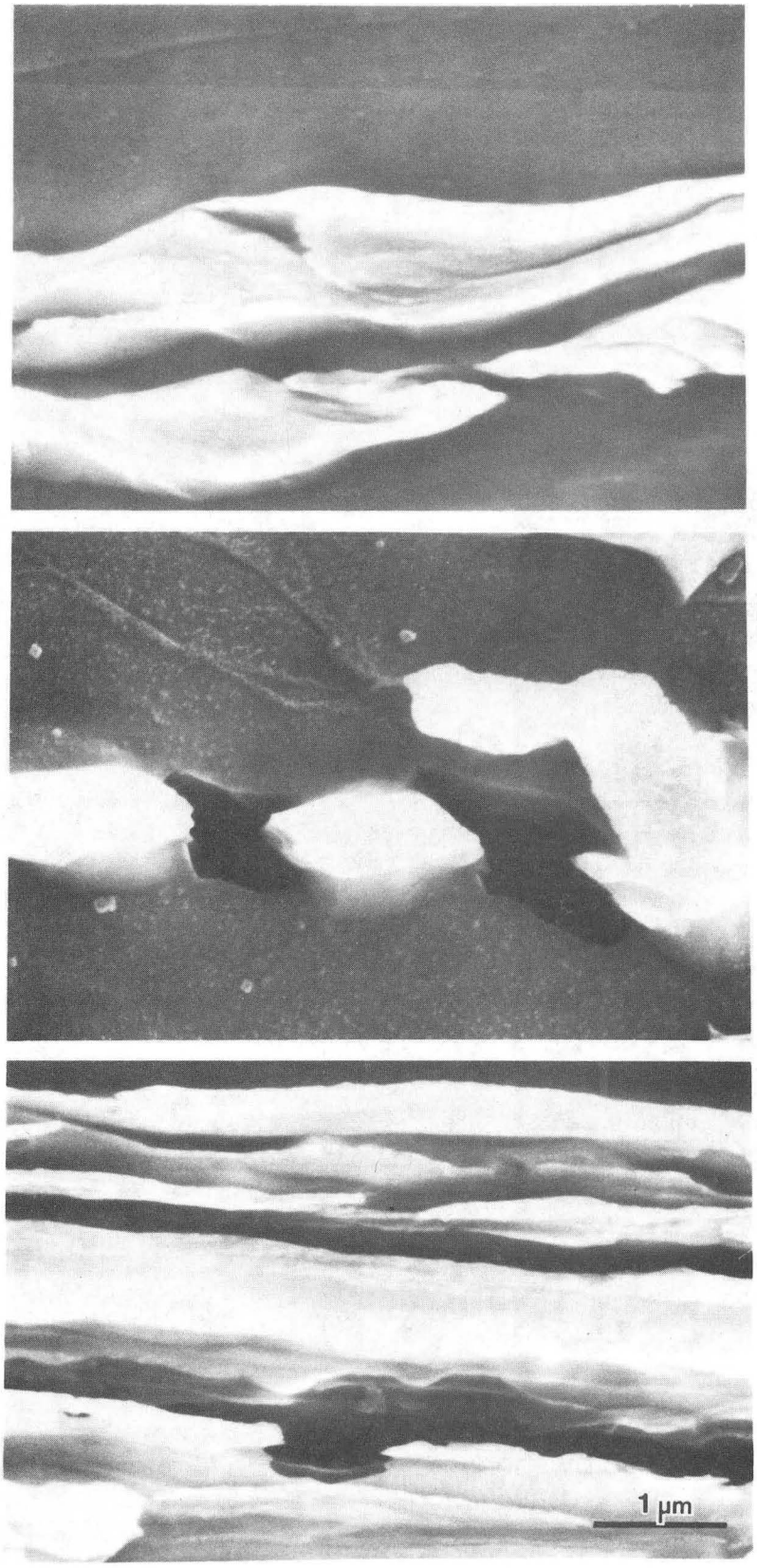

A. Shear Cracking

B. Void Growth

C. Longitudinal Crack

XBB 878-6573

Fig 7

DRAWING LIMIT AND FRACTURE MODE

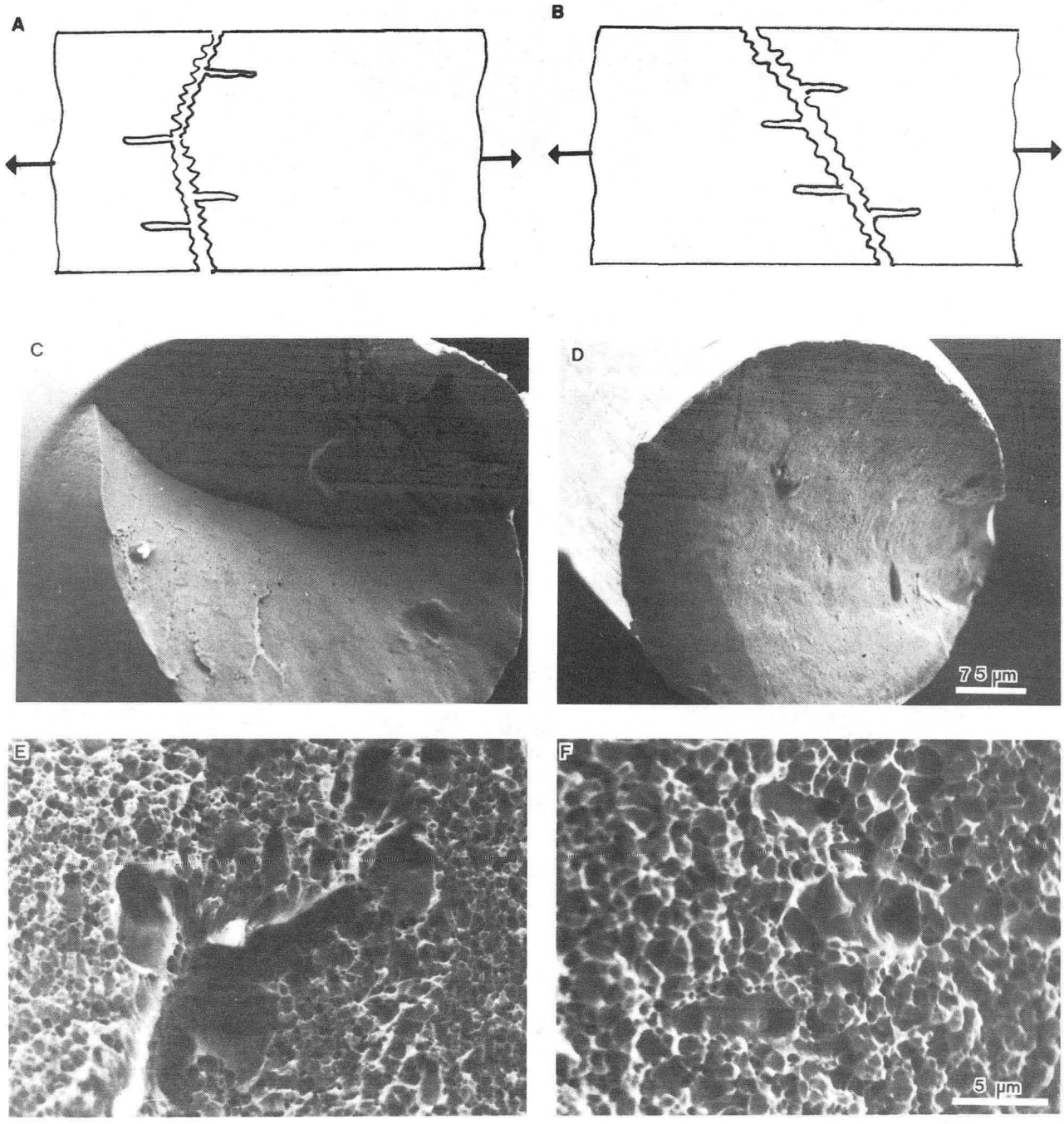

A,C,E-- V-slant fracture mode and B,D,F -- 45 degree slant fracture mode caused by shear instability as an indication of drawing limit

XBB 875-3809B

Fig 8

LAWRENCE BERKELEY LABORATORY
TECHNICAL INFORMATION DEPARTMENT
UNIVERSITY OF CALIFORNIA
BERKELEY, CALIFORNIA 94720